Available online at www.sciencedirect.com
ScienceDirect
Carbohydrate Polymers 66 (2006) 97–103
Carbohydrate Polymers
www.elsevier.com/locate/carbpol

# Changes in pore size distribution during the drying of cellulose fibers as measured by differential scanning calorimetry

Sunkyu Park, Richard A. Venditti *, Hasan Jameel, Joel J. Pawlak

*Department of Wood and Paper Science, North Carolina State University, Raleigh, NC 27695-8005, USA*

Received 24 November 2005; received in revised form 20 February 2006; accepted 20 February 2006
Available online 12 June 2006

**Abstract**

Changes in pore size distribution during the drying of cellulose fibers were determined using differential scanning calorimetry (DSC) with an isothermal step melting procedure. Softwood bleached kraft pulp at various moisture ratios were generated from partial drying in a thermogravimetric analyzer and then analyzed in a DSC. The pore size distribution was calculated using the Gibbs–Thomson equation and specific melting point depression of water detected by DSC. It was observed that larger pores collapse first followed by the sequential collapse of smaller pores. It is suggested that pore wall collapse resistance is the primary factor that determines which size pores close. The average measured pore size in the fiber wall of the never dried fiber was calculated to be about 80 nm and reduced with drying of the fibers. A constant pore size of about 20 nm was observed at moisture ratios below 0.3 g/g, which corresponds to one-to-two layers of non-freezing bound water tightly bound to the surface.


*Keywords:* Cellulose fibers; Differential scanning calorimetry; Pore closure; Pore size distribution

## 1. Introduction

Pore properties such as pore shape, pore volume, and pore size distribution are important features of all porous media. These parameters affect the swelling capability that is directly related to mechanical and optical properties of non-woven materials made from the cellulose fibers. These are also of interest in studying the accessibility of the cell walls to enzymes or other reactants. Pores in cellulose fibers are already present in nature and can be generated during chemical and mechanical treatments. Pulping and bleaching processes liberate lignin and hemicellulose from the fibers and as a result generate pores. Lignin and hemicellulose contents are about 25% and 30% by weight of wood, respectively. Refining of fibers, which fibrillates the surface by compressing and shearing actions, can also create pores within the cellulose fibers (Maloney & Paulapuro, 1999).

Pore analysis is not straightforward and difficult to define by a single number. For a complete analysis, pore dimension, geometry, topology, connectivity, and number of isolated pores should be considered. This, however, is not realistic and, in many cases, pores are assumed to be cylindrical in shape. Based on this, pore size distribution has been determined by various methods.

Measurement techniques include mercury intrusion (Chu & Kimura, 1996; Rigby, Fletcher, & Riley, 2002), gas permeability (Carey, Leekley, Hultman, & Nagel, 1973), scanning electron microscopy (Chinga, Helle, & Forseth, 2002), atomic force microscopy (Mohammad, Hilal, & Seman, 2005), and light scattering (Springer, Raether, Caps, & Manara, 2000). These methods have been successfully applied to certain types of porous materials, but there are limitations to cellulose fibers. First, these techniques require dried samples for the measurements. However, the pores in the cellulose fibers are significantly altered upon drying. This is the well-known phenomenon of hornification (Weise, 1998; Welf, Venditti, Hubbe, & Pawlak, 2005; Wistara & Young, 1999; Zhang, Hubbe,

* Corresponding author.
*E-mail address:* richard_venditti@ncsu.edu (R.A. Venditti).

0144-8617/$ - see front matter © 2006 Elsevier Ltd. All rights reserved.
doi:10.1016/j.carbpol.2006.02.026

Venditti, & Heitmann, 2004), which describes the physical and chemical changes to cellulose fibers during drying and wetting. It is known that drying causes an irreversible physical contraction of the fiber cell wall, and thus a cellulose fiber swells to a much lower extent after it has been dried. Second, some of these techniques are conducted in a destructive manner. For the mercury intrusion method, the pressures required to fill pores are excessively high and the accuracy of the method reduces with the increased pressure. For scanning electron microscopy, pore structure is unnecessarily changed if samples are cut. Thus, for various reasons, these methods may possibly lead to inaccurate determinations of the pore size distribution in cellulose fibers.

A solute exclusion technique (Stone & Scallan, 1968) can be considered, which is undertaken in the swollen state. By using a series of different size molecular probes, which do not interact with the fibers, the distribution of accessible pores was calculated (Stone, Treiber, & Abrahamson, 1969). However, pores with very small entrances and isolated pores are not detected, leading to incorrect pore volume. The same principle is applied to inverse size-exclusion chromatography to measure the distribution of pores in the fibers (Berthold & Salmen, 1997; Keim, Li, Ladisch, & Ladisch, 2002). Since the fibers are evaluated under the fully swollen state, these methods are not appropriate for studying the drying behavior of the fibers.

A differential scanning calorimetry (DSC) method can be used to investigate the pore size distribution of cellulose fibers at different moisture ratios. From the DSC experiments, water absorbed in hydrophilic materials is categorized as non-freezing bound water, freezing bound water, and unbound water (Liu & Yao, 2001; Nakamura, Hatakeyama, & Hatakeyama, 1981; Ping, Nguyen, Chen, Zhou, & Ding, 2001). Non-freezing bound water is the first 1–3 layers of water adjacent to a surface and does not freeze because the motion of water structures is severely limited by the association with the surfaces (Berlin, Kliman, & Pallansch, 1970). Freezing bound water has thermodynamically different behavior than unbound water. The quantity of freezing bound water could be determined by the integration of either an exotherm (crystallization of water) or an endotherm (melting of water) (Nakamura et al., 1981; Sakabe, Ito, Miyamoto, & Inagaki, 1987). However, freezing bound water is generally characterized by the integration of the endotherm since the exothermic curve may not be detected during cooling in some cases (Hori, Zhang, & Shimizu, 1988; Yamauchi & Murakami, 1991).

Water held in the capillaries of porous materials has a depressed melting temperature because of the lower pressure at a curved interface in cavities. The melting temperature depression has a reciprocal relationship with the pore diameter and thus the pore size distribution can be evaluated. This is the principle of thermoporometry based on the phenomenon called freezing point depression. A detailed theoretical basis for this method was established (Brun, Lallemad, Quinson, & Eyraud, 1977; Burghoff & Pusch, 1979). This method has been applied to cellulose fibers with an isothermal step melting procedure (Maloney, Paulapuro, & Stenius, 1998; Maloney & Paulapuro, 1999) and found to be in good agreement with other methods such as NMR cryoporometry and mercury intrusion (Gane et al., 2004).

In this study, changes in the pore size distribution of cellulose fibers were determined as a function of the moisture ratio using a series of isothermal step melting sequences in a DSC.

## 2. Materials and methods

### 2.1. Samples

Softwood fully bleached kraft pulp after the bleaching stage was obtained from Weyerhaeuser (Plymouth, NC). This was a mixture of loblolly pine and southern pine. The pulp was never dried and used for all experiments. The fiber has an average length of 2.56 mm (length weighted) and an average width of 30.0 μm measured by FQA (Fiber Quality Analyzer, OpTest Equipment Inc., Ontario, Canada).

### 2.2. Analytical instruments for thermal analysis

A thermogravimetric analyzer (Q500 TGA, TA Instruments) was used to dry the samples partially and to measure the weight of the DSC sample. A differential scanning calorimeter (Q100 DSC, TA Instruments) equipped with a cooling unit (RCS, Refrigerated Cooling System) was used to measure the pore size distribution and the bound water content of the fibers of different moisture ratios.

Fully saturated fibers were introduced into the furnace of the TGA. The fibers were isothermally dried at 90 °C and the drying was interrupted at different times to produce samples with different moisture ratios. Then, the samples of approximately 5.0 mg were sealed into a DSC aluminum hermetic pan (TA Instruments, Part #900793.901 for bottom and Part #900794.901 for lid) for evaluating the pore size distribution and the bound water content. After completing the DSC measurements, the sample pans were reweighed to check if water had escaped during the experiment. To measure the dried weight of the fibers, the lids were punctured and then dried in the TGA at 110 °C until the weight did not change.

### 2.3. Temperature calibration

Temperature calibration of the DSC was performed using approximately 5 mg of ultra pure water (Milli-Q system, Millipore Corporation). The water pan was cooled to −30 °C and the temperature was maintained for 5 min to ensure that all of the water was frozen. After that, the pan was heated to 10 °C at a heating rate of 1 °C/min. It is important to use the same heating rate throughout the

experiments; otherwise the results are influenced by the heating rate. This is discussed in this paper. The temperature at which the ice starts to melt was calibrated to 0.00 °C (onset of the melting peak). Several runs were conducted and it was found that the temperature reproducibility was about ±0.02 °C.

### 2.4. Measurement of freezing and non-freezing bound water

Freezing bound water was measured by two different DSC program modes: a continuous melting and an isothermal step melting sequence. In the first method, the sample pan was cooled to −30 °C and scanned at 1 °C/min to 15 °C. Overlapping peaks for freezing bound water and unbound water were separated by splitting the integrated areas of heat flow at the temperature of inflection between the peaks (Weise, Maloney, & Paulapuro, 1996). In the second method, freezing bound water is the total sum of the pore water from the isothermal step melting program. This isothermal step melting mode is explained in detail in the next section.

The amount of non-freezing bound water was calculated by subtracting the total freezable water (both freezing bound water and unbound water) in the sample (determined from integration of DSC thermogram) from the moisture ratio in the initial sample (determined gravimetrically using TGA microbalance).

### 2.5. Measurement of pore size distribution

Pore size distribution was determined by measuring the amount of water that has its melting temperature depressed at each isothermal step procedure. The samples were cooled to −30 °C and maintained for 5 min and the temperature was then raised to −20 °C at 1 °C/min. This first segment (−30 to −20 °C) was used to determine the sensible heat of the wet fibers, assuming that there was no melting. Subsequent heating steps to slightly higher temperatures (−15, −10, −6, −4, −2, −1.5, −1.1, −0.8, −0.5, −0.2, and −0.1 °C) were then performed in succession. In each step, the temperature was raised at 1 °C/min to the target temperature and then the sample was maintained isothermally until the heat flow returned to the baseline value. An example of the isothermal step melting program and the resulting heat flow is shown in Fig. 1. The heat absorbed during the heating and isothermal time period was calculated by integrating the endotherm. Thus, a melting enthalpy ($H_m$) is calculated by subtracting a sensible heat ($C_p \cdot \Delta T$) from a total heat ($H_t$) for each segment as shown in Eq. (1)

$$H_m = H_t - C_p \cdot \Delta T. \quad (1)$$

The relationship between a pore diameter ($D$) and the depressed melting temperature ($T_m$) is described by Eq. (2) (Furó & Daicic, 1999), which reduces to the Gibbs–Thomson equation when the contact angle is assumed to be 180° (Skapski, Billups, & Rooney, 1957). The use of Eq. (2) is based on the assumption that the cellulose is not soluble in the water and its pore shape is cylindrical. Based on the equation, each melting temperature depression ($\Delta T$) represents a specific pore diameter as listed in Table 1.

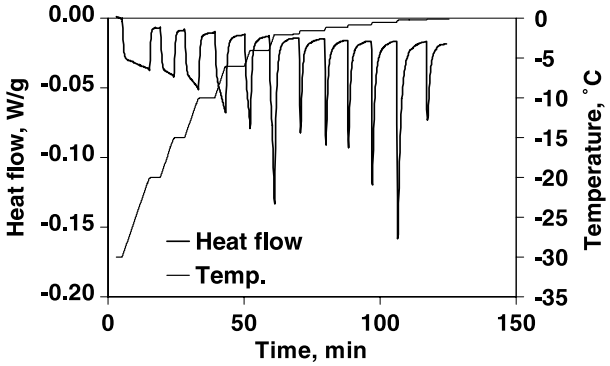


Fig. 1. The melting of water in fibers (moisture ratio of 0.83 g/g) during an isothermal step melting program. A negative heat flow indicates an endotherm.

$$\Delta T = T_0 - T_m = \frac{-4T_0\gamma_{ls}\cos\theta}{D\rho H_f}, \quad (2)$$

where $T_0$ is the melting temperature of water (273.15 K), $\gamma_{ls}$ is the surface energy at the ice-water interface (12.1 mJ/m$^2$) (Ishikiriyama, Todoki, & Motomura, 1995; Maloney & Paulapuro, 1999), $\rho$ and $H_f$ are the density and the specific heat of fusion of freezing bound water, respectively, assumed to be the same as that of unbound water (1000 kg/m$^3$, 334 J/g) (Maloney, Paulapuro, & Stenius, 1998; Nakamura et al., 1981), $D$ is the diameter of the pore, and ΔT is the melting temperature depression (K). Thus, water held in a smaller pore has a larger melting temperature depression. It is acknowledged that real pores in fibers will be irregularly shaped and that Eq. (2) is a method of estimating effective pore diameters in fibers. Scanning electron microscopy has been used to provide details on the actual pore geometry and features (Alince, 2002).

Table 1
Relationship between the melting temperature depression and the pore diameter based on the Gibbs–Thomson effect, Eq. (2)

| $T_m$ (°C) | $D$ (nm) |
|---|---|
| −15 | 2.6 |
| −10 | 4.0 |
| −6 | 6.6 |
| −4 | 9.9 |
| −2 | 19.8 |
| −1.5 | 26.4 |
| −1.1 | 36.0 |
| −0.8 | 49.5 |
| −0.5 | 79.2 |
| −0.2 | 198 |
| −0.1 | 396 |

## 3. Results and discussion

### 3.1. Effect of heating rate on bound water content

Various heating rates have been used to determine freezing bound water: 1 °C/min (Yamauchi & Murakami, 1991), 2 °C/min (Yamauchi & Tamai, 2003), 5 °C/min (Hori et al., 1988; Maloney et al., 1998; Sakabe et al., 1987), and 8 °C/min (Nakamura et al., 1981). The influence of heating rate on the bound water content is shown in Fig. 2. Fully saturated fibers having the moisture ratio of 1.15 g/g were used. The amount of freezing bound water decreased with the increased heating rate: 0.347 g/g at 1 °C/min and 0.257 g/g at 5 °C/min. This may be due to the thermal delay of the melting transition. For the fast heating rate, unbound water could start to melt when freezing bound water does not completely melt. If true, it is considered that lower heating rates provide less convoluted data. Thus, the heating rate of 1 °C/min is used in the rest of this study.

Even though the heating rate of 1 °C/min is used, the melting temperature of freezing bound water in the fibers is depressed only slightly below that of unbound water. For this reason, the endothermic transitions are overlapped when a continuous melting method is used. This is due to the large average pore size of the fibers compared to other systems that have small pore size such as polyethylene glycol, regenerated cellulose films, and silica gels, for which melting transitions are not overlapped (Hay & Laity, 2000; Ishikiriyama et al., 1995; Yamauchi & Tamai, 2003).

Thus, overlapping transitions are separated by splitting the integrated areas at the point of inflection (Weise et al., 1996). The freezing bound water content measured by this method is compared with that measured by isothermal step melting method as shown in Fig. 3. The two different measurements show a strong correlation.

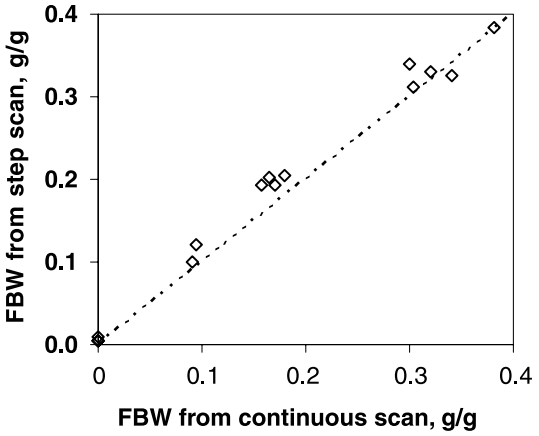


Fig. 3. Comparison of the freezing bound water (FBW) content between the continuous melting program and isothermal step melting program. The dotted line indicates a one-to-one relationship between the methods.

### 3.2. Effect of moisture ratio on bound water content

Bound water is thought to be held within small pores in the fibers and the amorphous regions of the cell walls composed of hemicellulose gel and/or amorphous cellulose. The content of bound water is not influenced by moisture ratios greater than 0.8 g/g, but decreases with drying for moisture ratios less than 0.8 g/g, Fig. 4. However, non-freezing bound water is relatively constant at moisture ratios greater than 0.3 g/g and decreases with further drying of the fibers. Freezing bound water can be observed as the difference between the bound water and the non-freezing bound water in Fig. 4. It is observed that there is only a small portion of freezing bound water remaining in the fibers at the moisture ratio of around 0.3 g/g, which corresponds to the moisture content (water mass divided by total sample mass) of 0.23 g/g in the fibers. From this result, the drying order of bound water is elucidated: freezing bound water is removed first followed by non-freezing bound water.

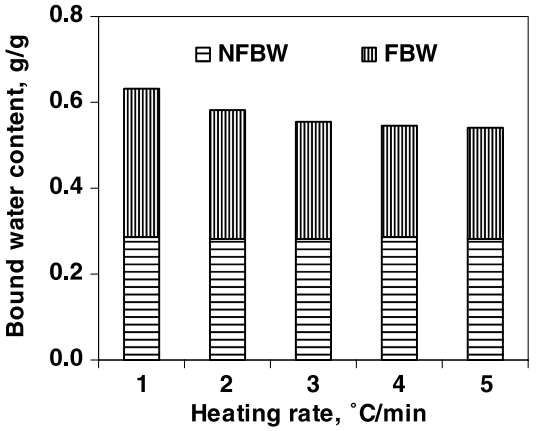


Fig. 2. Effect of the heating rate on the bound water content measured with the continuous melting procedure. Freezing bound water (FBW) decreased with the higher heating rate.

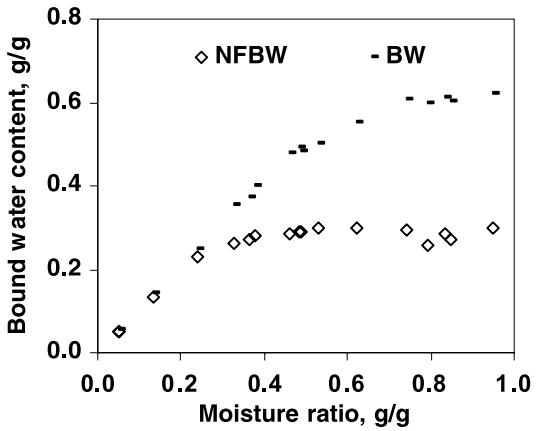


Fig. 4. Effect of moisture ratio on the bound water (BW) content in the fibers. Bound water includes freezing bound water and non-freezing bound water (NFBW).

### 3.3. Bound water in cellulose fibers

The bound water content of the fibers examined in this study is 0.63 g/g for moisture ratios greater than 0.8 g/g, Fig. 4. These same fibers were used in a previous study and it was found that a water retention value (moisture ratio of wet fibers after centrifugation) and a hard-to-remove water content (moisture ratio at onset point between constant rate isothermal drying zone and falling rate isothermal drying zone) were 1.9 and 1.5 g/g, respectively (Park, Venditti, Jameel, & Pawlak, 2005). Since these values are attempts to represent the fiber in a saturated state without excess water present, it can be concluded that a significant amount of the water contained in the saturated fibers has the same thermodynamic properties as that of unbound water. A likely interpretation is that unbound water is contained within larger pores such as networks and lumens of the fibers. For example, the size of lumen for this fiber is about 10 μm in diameter.

For the softwood bleached kraft fibers in this study, non-freezing bound water is determined to be about 0.28 g/g, Fig. 4. This result is consistent with the amounts of non-freezing bound water found for starches (Mausseri, Steinber, Nelson, & Wei, 1974) and wood fibers (Maloney et al., 1998). This amount is thought to be related to the number and type of the accessible hydration sites (Berthold, Rinaudo, & Salmen, 1996). The number of layers of non-freezing bound water adsorbed on the inner and outer surfaces of the cellulose fibers can be estimated based on a simple model as shown in Eq. (3). The number of layers of water molecules is given by

$$\text{Number of water layer} = \frac{W_c M_m}{M_{water}} \cdot \frac{1}{S} \cdot \frac{1}{(1-C)}, \quad (3)$$

where $W_c$ is the non-freezing bound water content (0.28 g/g). $M_m$ and $M_{water}$ are the molecular weight of repeating unit (162) and water (18), respectively. $S$ is the maximum bonding sites in a monomer (equal to 3) and $C$ is the crystallinity of fibers (taken as 44% (Nakamura et al., 1981)). It is estimated from Eq. (3) that one-to-two layers of water are adsorbed on fiber surfaces. Thus, the one-to-two layers of non-freezing bound water are associated with the surfaces to the extent that they are bound tightly to the surface and are not freezable (Berlin et al., 1970). This result is in good agreement with an adsorption model for lingo-cellulose materials (Berthold et al., 1996). It is appropriate to count non-freezing bound water as a part of the pore water because most of the surface area is considered to be located in the pores of the fibers.

### 3.4. Changes in pore size distribution of fibers

With the drying of fibers, water is evaporated from the pores and the pores collapse due to the capillary forces with the high surface tension of water. When the water starts to leave the pore, a very low pressure can exist in the water left in the pores, pulling the cell wall together as shown in Fig. 5. This is known as pore closure in the cellulose fibers during drying. It is possible to utilize the DSC isothermal step melting procedure to track the pore closure of different pore sizes. The cumulative bound water content versus pore diameter, neglecting the thickness of the non-freezing bound water, is shown in Fig. 6. The pore size distribution from this method was found to be nearly independent of moisture ratios for values greater than 0.8 g/g, data not shown here. From the results of several samples with moisture ratios less than 0.8 g/g, it was found that the fiber wall begins to collapse starting with larger pores (e.g., greater than 100 nm in diameter) followed by the sequential collapse of smaller pores (e.g., smaller than 10 nm in diameter). After reaching a certain moisture ratio due to the drying of the fibers, the distribution curve becomes flat, indicating that there is no freezable water remaining (between MR 0.33 and MR 0.13 in Fig. 6). The flat distribution further decreases with decreased moisture ratio as the non-freezing bound water is reduced.

Which pores collapse depends on two primary factors. First, the size of the pores affects the internal pressure of the pore liquid. Smaller pores will have smaller radii of curvature, generating lower pressures within the pore liquid and thus larger pore closure forces. The second factor is the ability of the pore wall to resist collapse. Larger pores should have less resistance in collapse. In fact the collapsing pressure of a tube is related to the inverse of the tube diameter (Marks, 1941). From the findings indicating that the large pores collapse first, it is suggested that the pore wall resistance is the governing factor and the different

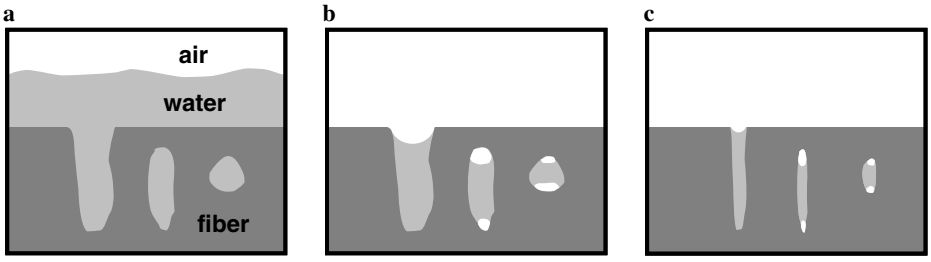


Fig. 5. Conceptual model of pore closure. When water is evaporated (a → b → c), surface tension pulls the cell wall together and the pore size becomes smaller.

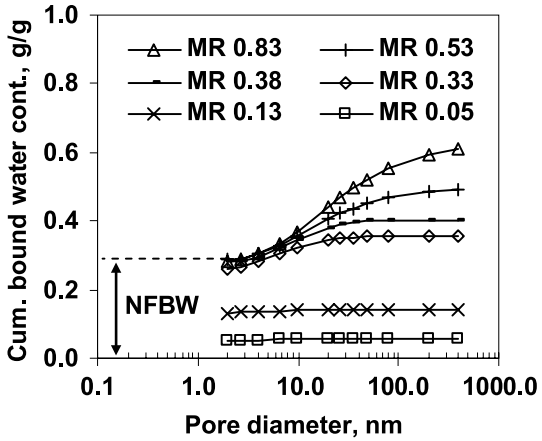


Fig. 6. The cumulative bound water content versus pore diameter at different moisture ratios.

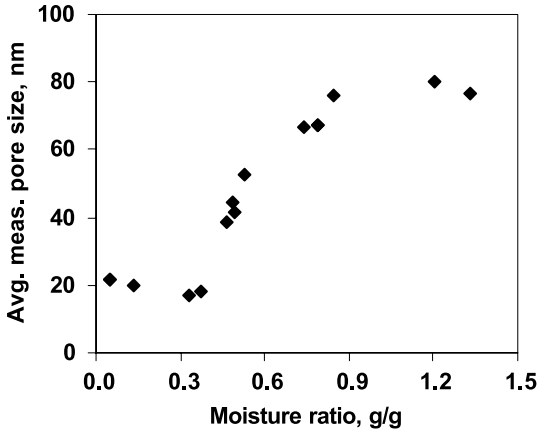


Fig. 7. Effect of moisture ratio on the average measured pore size of the fibers.

internal pressure generated in the different pore sizes is of secondary importance.

It is worth noting a limitation of this method. The maximum pore diameter of 396 nm in Table 1 is calculated from the depression temperature of −0.1 °C. A pore diameter of 3.96 μm could be detected if the equipment was sensitive to depression temperatures of −0.01 °C. However, in the experience of the authors with this equipment, the depression temperature of −0.1 °C was the practically closest temperature below the freezing point, 0.00 °C, which could be utilized in this study. This is important because it appears that, for moisture ratio of 0.83 g/g, there is no plateau in the pore diameter distribution for large ranges, indicating that there is a significant amount of pores larger than 396 nm present in the fiber. These larger pores are expected to be present and originating from both nm scale features (as mostly captured in Fig. 6) and μm scale features such as the lumen of fibers, fiber pits, fiber cracks and the inter-fiber pores developed from the geometry of the fiber network. For the samples with moisture ratio of 0.38 g/g and less, there is a plateau in the pore diameter distribution for the detected large pores, indicating that the large pores (at least those with nm scale features) have already collapsed on drying.

The average measured pore size was calculated from the data in Fig. 6 and is shown in Fig. 7. The average measured pore size is reduced with the drying of the fibers. At the moisture ratio below 0.3 g/g, the average pore size is not reduced any more, but a constant value of about 20 nm is realized. This point in drying roughly corresponds to a moisture ratio at which there is only non-freezing bound water present in the fibers.

The average measured pore size of 80 nm for moisture ratios greater than 0.8 g/g determined herein is consistent with SEM micrographs of freeze dried fibers of 100 nm (Duchesne & Daniel, 1999) and a benzene desorption isotherm study of 100 nm (Alince, 2002), but is considerably larger than that from solute exclusion of less than 30 nm (Stone & Scallan, 1968). This is considered due to the fundamental differences between the measuring techniques. Solute exclusion often underestimates the pore size due to its inability to detect isolated pores and pores with small entrances (Alince, 2002).

## 4. Conclusion

Differential scanning calorimetry (DSC) was used to investigate the bound water content and the pore size distribution of cellulose fibers with various moisture ratios. It was found that the bound water content was constant for moisture ratios greater than 0.8 g/g and decreased with drying for moisture ratios less than 0.8 g/g. It was also observed that the non-freezing bound water content was constant for moisture ratios greater than 0.3 g/g and decreased with decreasing moisture ratio below. This demonstrates that freezing bound water is removed first during the drying of cellulose fibers followed by non-freezing bound water. Based on a simple model used in this study, non-freezing bound water corresponds to one-to-two layers of water tightly bound to the surface.

Changes in the pore size distribution during the drying of cellulose fibers were determined with an isothermal step DSC melting procedure. It was found that the fiber wall begins to collapse starting with larger pores followed by the sequential collapse of smaller pores. Analysis of the pore size distribution curve confirms that below 0.3 g/g moisture ratio only non-freezing bound water exists (with no freezing bound water remaining). From these findings, it is suggested that the pore wall resistance to collapse is the primary reason for pore closure and that the pressure difference generated from different pore sizes is a secondary factor.

The average measured pore size was calculated to be about 80 nm for moisture ratios greater than 0.8 g/g and this is reduced upon further drying of the fibers. At a moisture ratio below 0.3 g/g, a constant pore size of about 20 nm was observed. This point in drying roughly corresponds to a moisture ratio at which there is only non-freezing bound water present in the fibers.

## References


Alince, B. (2002). Porosity of swollen pulp fibers revisited. *Nordic Pulp and Paper Research Journal, 17*(1), 71–73.

Berlin, E., Kliman, P. G., & Pallansch, M. J. (1970). Changes in state of water in proteinaceous systems. *Journal of Colloid Interface Science, 34*(4), 488–494.

Berthold, J., Rinaudo, M., & Salmen, L. (1996). Association of water to polar groups: Estimations by an adsorption model for lingo-cellulosic materials. *Colloids and Surfaces A, 112*(2-3), 117–129.

Berthold, J., & Salmen, L. (1997). Inverse size exclusion chromatography (ISEC) for determining the relative pore size distribution of wood pulps. *Holzforschung, 51*(4), 361–368.

Brun, M., Lallemad, A., Quinson, J. F., & Eyraud, C. (1977). New method for simultaneous determination of size and shape of pores—thermoporometry. *Thermochimica Acta, 21*(1), 59–88.

Burghoff, H. G., & Pusch, W. (1979). Characterization of water structure in cellulose acetate membranes by calorimetric measurements. *Journal of Applied Polymer Science, 23*(2), 473–484.

Carey, C. L., Leekley, R. M., Hultman, J. D., & Nagel, S. C. (1973). Determination of pore size distribution of pigment coatings. *Tappi Journal, 56*(11), 134–138.

Chinga, G., Helle, T., & Forseth, T. (2002). Quantification of structure details of LWC paper coating layers. *Nordic Pulp and Paper Research Journal, 17*(3), 313–318.

Chu, F., & Kimura, Y. (1996). Structure and gas permeability of microporous films prepared by biaxial drawing of beta-form polypropylene. *Polymer, 37*(4), 573–579.

Duchesne, I., & Daniel, G. (1999). The ultrastructure of wood fiber surfaces as shown by a variety of microscopical methods—A review. *Nordic Pulp and Paper Research Journal, 14*(2), 129–139.

Furó, I., & Daicic, J. (1999). NMR cryoporometry: A novel method for the investigation of the pore structure of paper and paper coatings. *Nordic Pulp and Paper Research Journal, 14*(3), 221–225.

Gane, P. A. C., Ridgway, C. J., Lehtinen, E., Valiullin, R., Furó, I., Schoelkopf, J., et al. (2004). Comparison of NMR cryoporometry, mercury intrusion porosimetry, and DSC thermoporosimetry in characterizing pore size distribution of compressed finely ground calcium carbonate structures. *Industrial and Engineering Chemistry Research, 43*(24), 7920–7927.

Hay, J. N., & Laity, P. R. (2000). Observation of water migration during thermoporometry studies of cellulose films. *Polymer, 41*(16), 6171–6180.

Hori, T., Zhang, H-S., & Shimizu, T. (1988). Change of water states in acrylic fibers and their glass transition temperature by DSC measurements. *Textile Research Journal, 58*(4), 227–232.

Ishikiriyama, K., Todoki, M., & Motomura, K. (1995). Pore size distribution measurement of silica gels by means of differential scanning calorimetry. *Journal of Colloid Interface Science, 171*(1), 92–102.

Keim, C., Li, C., Ladisch, C. M., & Ladisch, M. (2002). Modeling pore size distribution in cellulose rolling stationary phases. *Biotechnology Progress, 18*, 317–321.

Liu, W. G., & Yao, K. D. (2001). What causes the unfrozen water in polymers: Hydrogen bonds between water and polymer chains?. *Polymer 42*(8), 3943–3947.

Maloney, T. C., Paulapuro, H., & Stenius, P. (1998). Hydration and swelling of pulp fibers measured with differential scanning calorimetry. *Nordic Pulp and Paper Research Journal, 13*(1), 31–36.

Maloney, T. C., & Paulapuro, H. (1999). The formation of pores in the cell wall. *Journal of Pulp and Paper Science, 25*(12), 430–436.

Marks, L. S. (1941). *Mechanical engineers' handbook* (4th ed.). New York and London: McGraw-Hill Inc., pp. 449–451.

Mausseri, J., Steinber, M. P., Nelson, A. I., & Wei, L. S. (1974). Bound water capacity of corn starch and its derivatives by NMR. *Journal of Food Science, 39*(1), 114–116.

Mohammad, A. W., Hilal, N., & Seman, M. N. A. (2005). Interfacially polymerized nanofiltration membranes: Atomic force microscopy and salt rejection studies. *Journal of Applied Polymer Science, 96*(3), 605–612.

Nakamura, K., Hatakeyama, T., & Hatakeyama, H. (1981). Studies on bound water of cellulose by differential scanning calorimetry. *Textile Research Journal, 51*(9), 607–613.

Park, S., Venditti, R. A., Jameel, H., & Pawlak, J. J. (2005). Hard to remove water in cellulose fibers characterized by high resolution thermogravimetric analysis—method development. *Cellulose* (in print, available online).

Ping, Z. H., Nguyen, Q. T., Chen, S. M., Zhou, J. Q., & Ding, Y. D. (2001). State of water in different hydrophilic polymers—DSC and FTIR studies. *Polymer, 42*(20), 8461–8467.

Rigby, S. P., Fletcher, R. S., & Riley, S. N. (2002). Determination of the multiscale percolation properties of porous media using mercury porosimetry. *Industrial and Engineering Chemistry Research, 41*(5), 1205–1226.

Sakabe, H., Ito, H., Miyamoto, T., & Inagaki, H. (1987). States of water sorbed on wool as studied by differential scanning calorimetry. *Textile Research Journal, 57*(2), 66–72.

Skapski, A., Billups, R., & Rooney, A. (1957). Capillary cone method for determination of surface tension of solids. *Journal of Chemical Physics, 26*(5), 1350–1351.

Springer, R., Raether, F., Caps, R., & Manara, J. (2000). In situ measurement of light scattering in porous ceramics during sintering. *High Temperatures-High Pressures, 32*(4), 385–390.

Stone, J. E., & Scallan, A. M. (1968). A structural model for the cell wall of water swollen wood pulp fibers based on their accessibility to macromolecules. *Cellulose Chemistry and Technology, 2*, 343–358.

Stone, J. E., Treiber, E., & Abrahamson, B. (1969). Accessibility of regenerated cellulose to solute molecules of a molecular weight of 180 to $2 \times 10^6$. *Tappi Journal, 52*(1), 108–110.

Weise, U., Maloney, T., & Paulapuro, H. (1996). Quantification of water in different states of interaction with wood pulp fibers. *Cellulose, 3*(4), 189–202.

Weise, U. (1998). Hornification: Mechanisms and terminology. *Paperi Ja Puu, 90*(2), 110–115.

Welf, E. S., Venditti, R. A., Hubbe, M. A., & Pawlak, J. J. (2005). The effect of heating without water removal and drying on the swelling as measured by water retention value and degradation as measured by intrinsic viscosity of cellulose papermaking fibers. *Progress in Paper Recycling, 14*(3), 5–13.

Wistara, N., & Young, R. A. (1999). Properties and treatments of pulps from recycled paper: Part I Physical and chemical properties of pulps. *Cellulose, 6*(4), 291–324.

Yamauchi, T., & Murakami, K. (1991). Differential scanning calorimetry as an aid for investigating the wet state of pulp. *Journal of Pulp and Paper Science, 17*(6), 223–226.

Yamauchi, T., & Tamai, N. (2003). A novel approach using differential scanning calorimetry to investigate the dissolved state in aqueous solutions of polymers used for papermaking. *Journal of Applied Polymer Science, 89*(10), 2798–2807.

Zhang, M., Hubbe, M. A., Venditti, R. A., & Heitmann, J. A. (2004). Effects of sugar addition before drying on the wet flexibility of redispersed kraft fibers. *Journal of Pulp and Paper Science, 30*(1), 29–34.